Available online at www.sciencedirect.com
SCIENCE DIRECT®
Journal of Sound and Vibration 284 (2005) 893–914
JOURNAL OF SOUND AND VIBRATION
www.elsevier.com/locate/jsvi

# Period-one motions of a mechanical oscillator with periodically time-varying, piecewise-nonlinear stiffness

Qinglong Ma, A. Kahraman*

*Department of Mechanical Engineering, The Ohio State University, Columbus, OH 43210-1107, USA*

Received 12 February 2004; received in revised form 9 July 2004; accepted 20 July 2004
Available online 2 December 2004

**Abstract**

The dynamic behavior of a piecewise-nonlinear mechanical oscillator with parametric and external excitations is investigated. The viscously damped single-degree-of-freedom oscillator is subjected to a periodically time-varying, piecewise-nonlinear restoring function defined by a clearance surrounded by continuously nonlinear (quadratic and cubic) regions. Typical applications represented by this oscillator are highlighted. A multi-term harmonic balance formulation is used in conjunction with discrete Fourier transforms and a parametric continuation scheme to determine steady-state period-1 motions of the system due to both parametric and external excitations. The accuracy of the analytical solutions is demonstrated by comparing them to direct numerical integration solutions. Floquet theory is applied to determine the stability of the steady-state harmonic balance solutions. At the end, detailed parametric studies are presented to quantify the combined influence of clearance, quadratic and cubic nonlinearities within reasonable ranges of all other system parameters. A comparison between time-varying and time-invariant systems is also provided to demonstrate the influence of the parametric and external excitations on a piecewise-nonlinear system.
© 2004 Elsevier Ltd. All rights reserved.

## 1. Introduction

In this paper, the period-1 response of a single-degree-of-freedom (SDOF) oscillator with a unit mass is studied. The oscillator is subjected to viscous damping and a complex restoring function

*Corresponding author. Tel.: +1 614 292 4678; fax: +1 614 292 3163.
*E-mail address:* kahraman.1@osu.edu (A. Kahraman).

0022-460X/$ - see front matter © 2004 Elsevier Ltd. All rights reserved.
doi:10.1016/j.jsv.2004.07.026

$g[u(\tau)]$ that is formed by a combination of clearance and continuous nonlinearities. The system is excited by a periodically time-varying stiffness $w(\tau)$ and an external force $f(\tau)$ acting directly on the unit mass. In dimensionless form, the equation of motion for the oscillator is given by

$$\ddot{u}(\tau) + 2\zeta\dot{u}(\tau) + w(\tau)g[u(\tau)] = f(\tau), \tag{1}$$

where $\tau$ is the dimensionless time, an overdot denotes differentiation with respect to $\tau$, $u(\tau)$ is the displacement of the unit mass, and $\zeta$ is the viscous damping ratio. In Eq. (1), the piecewise-nonlinear (PN) function $g[u(\tau)]$ governs the dynamics of several mechanical systems, such as a splined disk–shaft interface [1], a sphere–plane contact [2–6], a rotor supported by rolling element bearings [7,8], spur gear pairs, and certain types of clutches and couplings.

Another critical feature of Eq. (1) is the periodically time-varying stiffness $w(\tau)$. In the case of a rolling element bearing, the total number of rolling elements (balls or cylindrical rollers) in contact fluctuates between two integers $P = m$ and $m + 1$ as the roller cage rotates. Similarly, in a spur gear pair, the overall number of loaded tooth pairs typically alternates between 1 and 2. In both applications, such rotation-dependent (and hence time-dependent) changes cause the overall stiffness at the interface to vary periodically, which is represented by $w(\tau)$ in Eq. (1).

Previous published studies on similar systems can be classified into two groups based on the stiffness function considered: (1) time-invariant (TI) systems with $w(\tau) = 1$ as in sphere–plane and spline joint examples, and (2) time-varying (TV) systems with periodic $w(\tau)$ as in the gear pair and rolling element bearing examples. In addition, based on the form of $g[u(\tau)]$, previous models fall into three categories: (1) continuously nonlinear (CN) with no clearance, (2) piecewise-linear (PL), and (3) piecewise-nonlinear (PN). By combining these two classifications, six individual groups can be formed, each of which uses a special version of Eq. (1) as listed in Table 1. In this table, a general PN form of $g[u(\tau)]$ is considered as

$$g[u(\tau)] = \begin{cases} \sum_{i=1}^{3} \alpha_i [u(\tau) - 1]^i, & u(\tau) > 1, \\ 0, & -1 \leqslant u(\tau) \leqslant 1, \\ \sum_{i=1}^{3} (-1)^{i-1} \alpha_i [u(\tau) + 1]^i, & u(\tau) < -1. \end{cases} \tag{2}$$

As Fig. 1 shows for different values of $\alpha_2$ and $\alpha_3$, $g[u(\tau)]$ consists of three segments: a clearance (dead-zone) segment for $u(\tau) \in [-1, 1]$, and two continuously nonlinear segments for $u(\tau) > 1$ and $u(\tau) < -1$. The nonlinear segments are defined by a linear stiffness component of slope $\alpha_1$, a quadratic nonlinearity term with coefficient $\alpha_2$, and a cubic nonlinearity term with coefficient $\alpha_3$.

As listed in Table 1, continuously nonlinear models (continuous nonlinear time-invariant (CNTI) and continuous nonlinear time-varying (CNTV)) have been studied extensively by using both numerical methods and well-established analytical techniques such as perturbation methods (e.g. Refs. [9–18]). Both softening- and hardening-type behavior were predicted for such systems as well as subharmonic, superharmonic and combination resonances. A full array of nonlinear phenomena were predicted and described thoroughly for such systems. On the other hand, PL systems (piecewise-linear time-invariant (PLTI) and piecewise-linear time-varying (PLTV)) have also been the focus of many studies, which demonstrated softening-type resonance peaks due to contact loss, and defined the conditions for the occurring of single- and double-sided impacts

Table 1
Different limiting cases of Eq. (1) with corresponding forms of $g[u(\tau)]$ and examples of previous studies

| Model type | Abbreviation | $w(\tau)$ | $g[u(\tau)]$ | Example Refs. |
|---|---|---|---|---|
| Continuous nonlinear, time-invariant | CNTI | Constant | $\sum_{i=0}^{n} \alpha_i u^i$ | [9–13] |
| Continuous nonlinear, time-varying | CNTV | Periodic | | [14–18] |
| Piecewise-linear, time-invariant | PLTI | Constant | $\begin{cases} u-1, & u>1, \\ 0, & -1\leqslant u\leqslant 1, \\ u+1, & u<-1. \end{cases}$ | [19–30] |
| Piecewise-linear, time-varying | PLTV | Periodic | | [31–41] |
| Piecewise-nonlinear, time-invariant | PNTI | Constant | $\begin{cases} \sum_{i=1}^{n} \alpha_i (u-1)^i, & u>1, \\ 0, & -1\leqslant u\leqslant 1, \\ \sum_{i=1}^{n} (-1)^{i-1} \alpha_i (u+1)^i, & u<-1. \end{cases}$ | [2–6,42–47] |
| Piecewise-nonlinear, time-varying | PNTV | Periodic | | — |

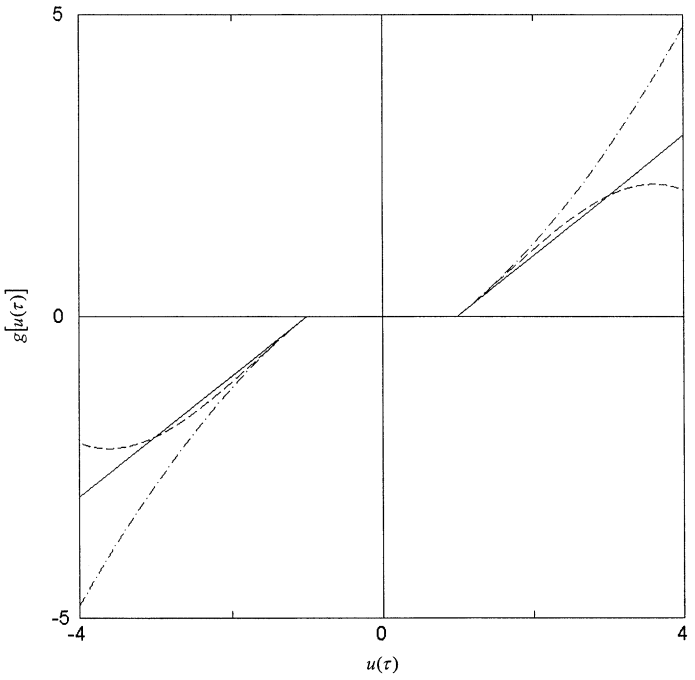


Fig. 1. Examples of restoring function $g[u(\tau)]$ given $\alpha_1 = 1$, and (- - -) $\alpha_2 = 0.2$, $\alpha_3 = -0.1$; (——) $\alpha_2 = \alpha_3 = 0$; and (- · · -) $\alpha_2 = 0.2$, $\alpha_3 = 0$.

(SSI and DSI) [19–41]. Moreover, for PLTV systems, it was shown that the regions of unstable solutions are bounded by stable subharmonic motions as a result of separations. Some of these predictions were also shown to match the experimental data well [31,32].

### 1.1. Objectives and scope

While a significant number of studies were performed on CN and PL systems with or without time-varying parameters, a limited number of published studies exist for PN systems, which combine both continuous and clearance nonlinearities. Most of these studies fall into the PNTI category [1–6,42–47] with constant stiffness coefficient. These studies mostly used numerical techniques with the exception of Refs. [46,47]. Meanwhile, the dynamic behavior of PNTV systems, as defined by Eqs. (1) and (2), is yet to be studied in detail. Accordingly, this paper focuses on the dynamic response of a SDOF PNTV oscillator governed by Eq. (1). Specific objectives are: (1) obtain the steady-state response analytically by using a multi-term harmonic balance method (HBM) in conjunction with discrete Fourier transforms (DFT), (2) demonstrate the accuracy of harmonic balance solutions by comparison to numerical integration results, (3) describe the impact of continuous nonlinearities of different types and magnitudes on the steady-state response of the PNTV systems, (4) quantify the influence of time-varying stiffness on the response through the comparison between the solutions of PNTI and PNTV systems, and (5) describe the effect of key system parameters such as damping ratio $\zeta$, alternating stiffness amplitude, preload $f_1$, and alternating external force amplitude on the dynamic response.

A parametric continuation scheme will be utilized for facilitating the solutions while passing through the turning points. Floquet theory will be employed for examining the stability of the steady-state motions. While the model proposed will be capable of finding period-$\eta$ subharmonic motions ($\eta > 1$) as well, only period-1 motions are presented in this paper. A companion paper will investigate subharmonic motions exhibited by the same system in detail [48].

## 2. Multi-term period-1 response to periodic excitations

A general method for obtaining steady-state period-1 solutions of Eq. (1) is presented in this section. This method combines a multi-term HBM formulation with DFT, which was applied to PL systems successfully [28–32]. Here $w(\tau)$ and $f(\tau)$ are written in the form of truncated Fourier series as

$$w(\tau) = 1 + \sum_{\kappa=1}^{K} [w_{2\kappa} \cos(\kappa \Lambda \tau) + w_{2\kappa+1} \sin(\kappa \Lambda \tau)], \tag{3a}$$

$$f(\tau) = f_1 + \sum_{\mu=1}^{M} [f_{2\mu} \cos(\mu \Lambda \tau) + f_{2\mu+1} \sin(\mu \Lambda \tau)], \tag{3b}$$

where $\Lambda$ is the dimensionless fundamental excitation frequency. $w_1 = 1$ is the mean component of the stiffness function, and $w_{2\kappa}$ and $w_{2\kappa+1}$ are the $\kappa$th harmonic amplitudes of $w(\tau)$. $f_1$ is the mean load (preload) applied to the unit mass, and $f_{2\mu}$ and $f_{2\mu+1}$ are the $\mu$th harmonic amplitudes of $f(\tau)$. $\kappa$ and $\mu$ are integer valued harmonic indices. By defining $\theta = \Lambda\tau$, Eq. (1) becomes

$$\Lambda^2 \frac{d^2u(\theta)}{d^2\theta} + 2\zeta\Lambda \frac{du(\theta)}{d\theta} + w(\theta)g[u(\theta)] = f(\theta). \tag{4}$$

The unknown steady-state period-1 response $u(\theta)$ and the PN restoring function $g[u(\theta)]$ can be expressed in Fourier series form as well:

$$u(\theta) = u_1 + \sum_{r=1}^{R} [u_{2r}\cos(r\theta) + u_{2r+1}\sin(r\theta)], \tag{5}$$

$$g[u(\theta)] = v_1 + \sum_{r=1}^{R} [v_{2r}\cos(r\theta) + v_{2r+1}\sin(r\theta)]. \tag{6}$$

While representing $g[u(\theta)]$ in Fourier series form seem unreasonable, the use of discrete Fourier transforms in determining its coefficients captures its piecewise properties properly [28–30] as it will be done later. By substituting Eqs. (3), (5) and (6) into Eq. (4) and enforcing harmonic balance, a vector equation $\mathbf{S} = \mathbf{0}$ is obtained in the following form:

$$S_1 = v_1 - f_1 + \frac{1}{2}\sum_{k=1}^{K} [w_{2k}v_{2k} + w_{2k+1}v_{2k+1}] = 0, \tag{7a}$$

$$\begin{aligned} S_{2r} = & -\Lambda^2 r^2 u_{2r} + 2\zeta\Lambda r u_{2r+1} + v_{2r} + v_1 w_{2r} - f_{2r} \\ & + \frac{1}{2}\sum_{k=1}^{K} w_{2k}[v_{2(k-r)} + v_{2(k+r)} + v_{2(r-k)}] \\ & + \frac{1}{2}\sum_{k=1}^{K} w_{2k+1}[v_{2(k-r)+1} + v_{2(k+r)+1} - v_{2(r-k)+1}] = 0, \quad r \in [1, R], \end{aligned} \tag{7b}$$

$$\begin{aligned} S_{2r+1} = & -\Lambda^2 r^2 u_{2r+1} - 2\zeta\Lambda r u_{2r} + v_{2r+1} + v_1 w_{2r+1} - f_{2r+1} \\ & + \frac{1}{2}\sum_{k=1}^{K} w_{2k}[-v_{2(k-r)+1} + v_{2(k+r)+1} + v_{2(r-k)+1}] \\ & + \frac{1}{2}\sum_{k=1}^{K} w_{2k+1}[v_{2(k-r)} - v_{2(k+r)} + v_{2(r-k)}] = 0, \quad r \in [1, R]. \end{aligned} \tag{7c}$$

The coefficients $v_i$ of $g[u(\theta)]$ can be expressed in terms of unknown Fourier coefficients of the response $\mathbf{u} = [u_1\ u_2\ u_3\ \ldots\ u_{2R}\ u_{2R+1}]^{\mathrm{T}}$ by utilizing the DFT [28,29,31,32]. The values of $u(\theta)$ at discrete values of $\theta = nh$ are

$$u_n = u_1 + \sum_{r=1}^{R}\left[u_{2r}\cos\left(\frac{2\pi rn}{N}\right) + u_{2r+1}\sin\left(\frac{2\pi rn}{N}\right)\right], \quad n \in [0, N-1], \tag{8a}$$

where $h = 2\pi/(N\Lambda)$ and $N \geqslant 2R$. Using Eq. (2), the $n$th discrete value of $g[u(\theta)]$ is given as

$$g_n = \begin{cases} \sum_{i=1}^{3} \alpha_i (u_n - 1)^i, & u_n > 1, \\ 0, & |u_n| \leqslant 1, \\ \sum_{i=1}^{3} (-1)^{i-1}\alpha_i (u_n + 1)^i, & u_n < -1 \end{cases} \tag{8b}$$

and the Fourier coefficients of $g[u(\theta)]$ are calculated by taking the inverse DFT of Eq. (8) as

$$v_1 = \frac{1}{N}\sum_{n=0}^{N-1} g_n, \quad v_{2r} = \frac{2}{N}\sum_{n=0}^{N-1} g_n \cos\frac{2\pi rn}{N}, \quad v_{2r+1} = \frac{2}{N}\sum_{n=0}^{N-1} g_n \sin\frac{2\pi rn}{N}. \tag{9a–c}$$

Having $v_i$, the vector equation $\mathbf{S} = \mathbf{0}$ can be solved for $\mathbf{u}$ by employing the Newton–Raphson method as

$$\mathbf{u}^{(m)} = \mathbf{u}^{(m-1)} - [\mathbf{J}^{-1}]^{(m-1)}\mathbf{S}^{(m-1)}, \tag{10}$$

where the value of $u^{(m)}$ at the $m$th iteration is obtained from the values of $\mathbf{S}^{(m-1)}$ and $\mathbf{u}^{(m-1)}$, and $\mathbf{J}$ is the Jacobian matrix. The Newton–Raphson iteration starts with an initial guess $\mathbf{u}^{(0)}$ and a control parameter that is chosen as $\Lambda$, and the process is repeated until the steady-state solution $\mathbf{u}^{(m)}$ converges within a predefined error limit. Then the control parameter is set to the next value of interest by increasing or decreasing $\Lambda$ until a turning point impedes continuation. In order to find the location of the turning point, the artificial-parameter generic homotopy method is utilized [49,50]. The iteration process is continued by using the value of the turning point as the new initial guess of the control parameter in the opposite incremental direction.

The stability of the steady-state response is determined by using Floquet theory [51]. Introducing a small variation $\Delta u(\tau)$ to the periodic solution $u_o(\tau) = u_o(\tau + T)$ where $T$ is the least period of $u(\tau)$, the following variational equation is obtained:

$$\Delta\ddot{u} + 2\zeta\Delta\dot{u} + \Psi(\tau)\tilde{g}[u_o(\tau)]\Delta u = 0, \tag{11a}$$

$$\tilde{g}[u_o(\tau)] = \begin{cases} \sum_{i=1}^{3} i\alpha_i[u_o - 1]^{i-1}, & u_o > 1, \\ 0, & |u_o| \leqslant 1, \\ \sum_{i=1}^{3} [-1]^{i-1} i\alpha_i[u_o + 1]^{i-1}, & u_o < -1. \end{cases} \tag{11b}$$

Defining $\mathbf{y} = [\Delta u(\tau)\ \ \Delta\dot{u}(\tau)]^{\mathrm{T}}$, Eq. (11a) is written in state-space form as $\dot{\mathbf{y}}(\tau) = \mathbf{H}(\tau)\mathbf{y}(\tau)$, where $\mathbf{H}(\tau) = \mathbf{H}(\tau + T)$ is the periodic state matrix. The variation of $\Delta u(\tau)$ during one minimal period can be determined by examining the eigenvalues of the monodromy matrix $\mathbf{\Phi} = \mathbf{Y}(T)$, and $\mathbf{\Phi}$ is obtained by solving $\dot{\mathbf{Y}}(\tau) = \mathbf{H}(\tau)\mathbf{Y}(\tau)$ given initial condition $\mathbf{Y}(0) = \mathbf{I}_2$, where $\mathbf{I}_2$ is an identity matrix of dimension 2. In this study, $\mathbf{\Phi}$ is computed by using the approximate method developed by Hsu and Cheng [52]. Finally, the local stability of $u_o(\tau)$ is determined by examining the eigenvalues of $\mathbf{\Phi}$. The solution is stable if the modulus of the eigenvalues is less than unity, and unstable otherwise.

### 2.1. Comparison to numerical integration results

A typical forced response is illustrated in Fig. 2 for an oscillator having a periodic stiffness function with $w_3 = 0.3$, $w_5 = 0.15$, $w_7 = 0.1$ $(K = 3)$, all other $w_i = 0$, and $\zeta = 0.05$. Here, the root-mean-square (rms) amplitude of the steady state response is defined as $u_{\mathrm{rms}} = \left[\sum_{r=1}^{R}(u_{2r}^2 + u_{2r+1}^2)\right]^{1/2}$. The piecewise-nonlinear function $g$ contains both quadratic and

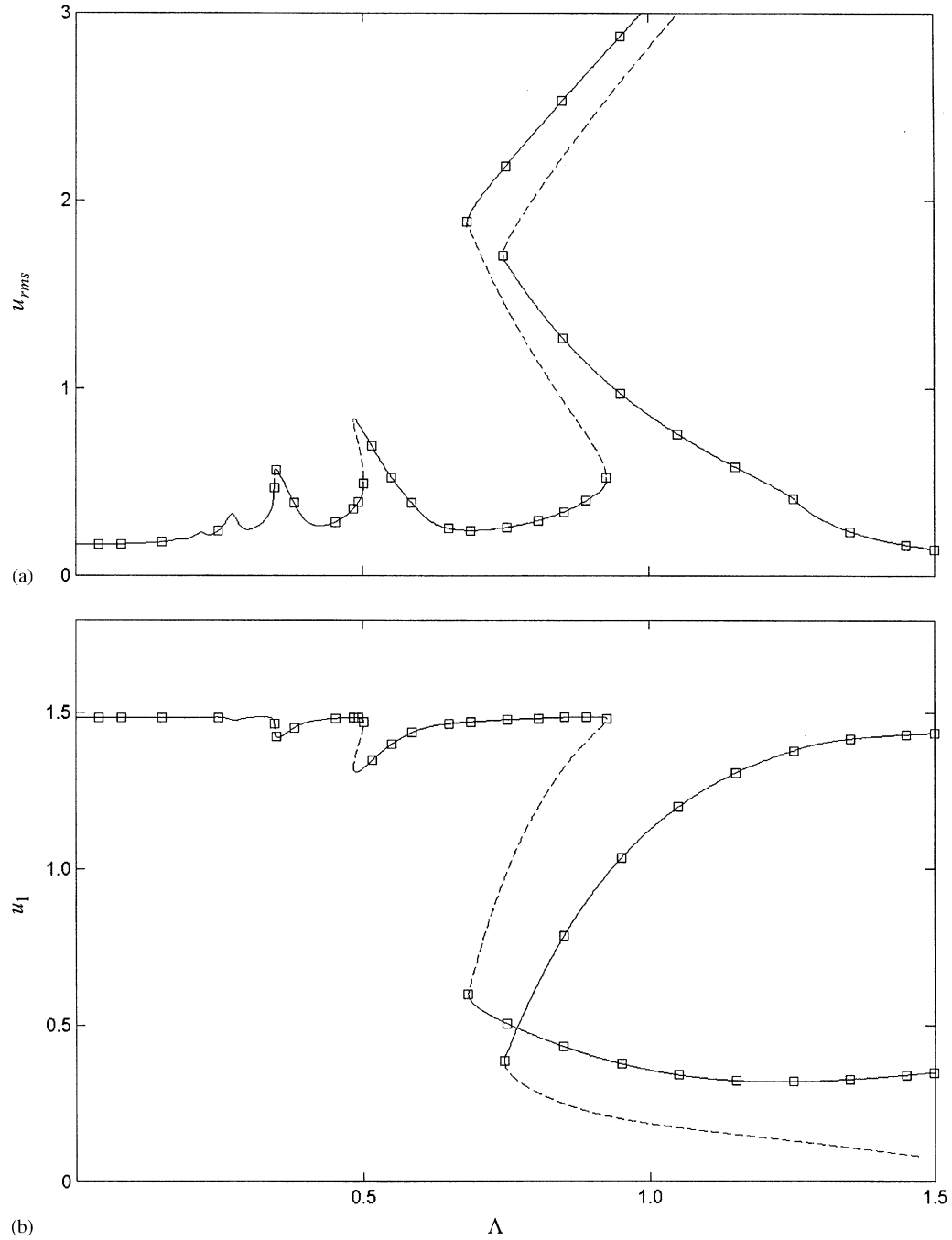


Fig. 2. (a) $u_{\text{rms}}$ and (b) $u_1$ values of forced response ($R = 6$) as a function of dimensionless frequency $\Lambda$ given $\alpha_2 = 0.1$, $\alpha_3 = 0.2, f_1 = 0.5, f_i = 0$ ($i \geqslant 2$), $w_3 = 0.3$, $w_5 = 0.15$, $w_7 = 0.1$ ($K = 3$), all other $w_i = 0$, and $\zeta = 0.05$. (—) stable HBM solutions, (– –) unstable HBM solutions, and (□) numerical integration solutions.

cubic coefficients $\alpha_2 = 0.1$, $\alpha_3 = 0.2$, in addition to a linear term $\alpha_1 = 1$. The oscillator is subjected to a mean load $f_1 = 0.5$ with no alternating external force ($f_i = 0, i = 2, 3, \ldots$). Fig. 2(a) shows the $u_{\text{rms}}$ values of both stable and unstable HBM solutions as a function of dimensionless frequency $\Lambda$. These solutions were obtained by considering six terms ($R = 6$) in Eq. (6). In addition, $u_{\text{rms}}$ obtained by direct numerical integration of Eq. (1) using backward differentiation formulas is shown in Fig. 2(a). Within each period, more than 2000 points were considered in the numerical integration to represent the transition times between the piecewise solution regimes reasonably well. A very good agreement is observed between the solutions from both methods. Similarly, the values of $u_1$ predicted by HBM and the numerical integration method compare well in Fig. 2(b) for the same case, further suggesting that the HBM solutions are indeed correct.

It is noted from Fig. 2(a) that, at $\Lambda \approx 0.9$, the stable (lower branch) solution loses its stability, causing a jump-up to another stable (upper branch) solution. Further examining these solutions in time domain indicates that the lower branch solution is such that $u(\tau) > 1$ for all $\tau$, which suggests that this motion is contained at the right piecewise segment of $g[u(\tau)]$, and the clearance nonlinearity has no influence on this motion. Using the same terminology introduced by Comparin and Singh [25], such motions will be called no-impact (NI) motions. NI motions will always take place in the right piecewise segment since the external force has a mean (preload) component forcing a contact in that segment. Similarly, $u(\tau) > -1$ for the upper branch solutions in Fig. 2(a) for $\Lambda$ from 1.25 back to 0.75, indicating that separation takes place. Here these motions are named as SSI motions that demonstrate a typical softening-type behavior due to contact loss. Finally, as the frequency is reduced at the upper branch, SSI motions lose their stability at $\Lambda \approx 0.75$. Either a jump-down to the lower branch NI motion or a jump-up to another stable motion is possible. These higher amplitude motions are such that $u(\tau) < -1$ for certain $\tau$, which indicates that these motions have back contacts following separations. The mass travels through the entire clearance region to initiate contact at the left piecewise segment. These motions will be called DSI motions.

## 3. Parametric studies

The parameter set for Eq. (1) is given as $P \in [\alpha_1, \alpha_2, \alpha_3, f_1, f_i, w_i, \zeta, \Lambda]$. Since the focus of the study is on the influence of clearance, quadratic ($\alpha_2$), and cubic ($\alpha_3$) nonlinearities, three cases are considered: (1) oscillators having clearance and cubic nonlinearities: $\alpha_1 = 1$, $\alpha_2 = 0$, and variable $\alpha_3$; (2) oscillators having clearance and quadratic nonlinearities: $\alpha_1 = 1$, $\alpha_3 = 0$, and variable $\alpha_2$; and (3) oscillators having all three types of nonlinearities: $\alpha_1 = 1$, and variable $\alpha_2$ and $\alpha_3$. Moreover, to limit the parametric study to a reasonable size, the influences of system parameters $f_1, f_i$, $w_i$ and $\zeta$ on the steady-state response are demonstrated only for case (1) in which $\alpha_1 = 1$, $\alpha_2 = 0$, and $\alpha_3$ has different values. The range of dimensionless frequency is defined as $\Lambda \in [0, 1.5]$. This range covers all primary and superharmonic resonance peaks of interest. Here the primary resonance frequency represents the undamped natural frequency of the corresponding linear system at $\Lambda = 1$ while the superharmonic resonances at $\Lambda = 1/\kappa$ ($\kappa \geqslant 2$) are due to the nonlinear effects [50]. In Eq. (6), the maximum index of Fourier series is chosen as $R = 6$, which has sufficient accuracy for the analysis, as shown in Fig. 2. Only $u_1$ and $u_{\text{rms}}$ values are used to represent $u(\tau)$ since the presentation of all harmonic amplitudes is not feasible. In all results

presented in the figures of the following sections, solid and dashed lines represent the stable and unstable period-1 motions, respectively.

### 3.1. $\alpha_1 = 1$, $\alpha_2 = 0$ *and variable* $\alpha_3$

In this case, $g[u(\tau)]$ is a PN function, which is formed by two nonlinear segments that are defined by a linear term $\alpha_1 = 1$ and a cubic nonlinear $\alpha_3$ term. The value of $\alpha_3$ is varied to obtain softening ($\alpha_3 < 0$) and hardening ($\alpha_3 > 0$) types of cubic nonlinearities. The case of $\alpha_3 = 0$ is also included to represent the corresponding PL system.

The effect of $f_1$ on the steady-state forced response for $\alpha_3 \neq 0$ is illustrated in Figs. 3 and 4 for $f_i = 0$ $(i \geqslant 2)$, $w_3 = 0.3$, $\zeta = 0.05$, $\alpha_1 = 1$, $\alpha_2 = 0$. The values of $\alpha_3$ and $f_1$ are varied, and the resultant changes on $u_{\mathrm{rms}}$ and $u_1$ of the system response are observed. In Figs. 3(a) and 4(a) for $f_1 = 0.25$, regardless of the value of $\alpha_3$, the motion is nearly linear for most $\Lambda$ except the range near $\Lambda = 1$, where a softening-type nonlinear response is formed by SSI solutions

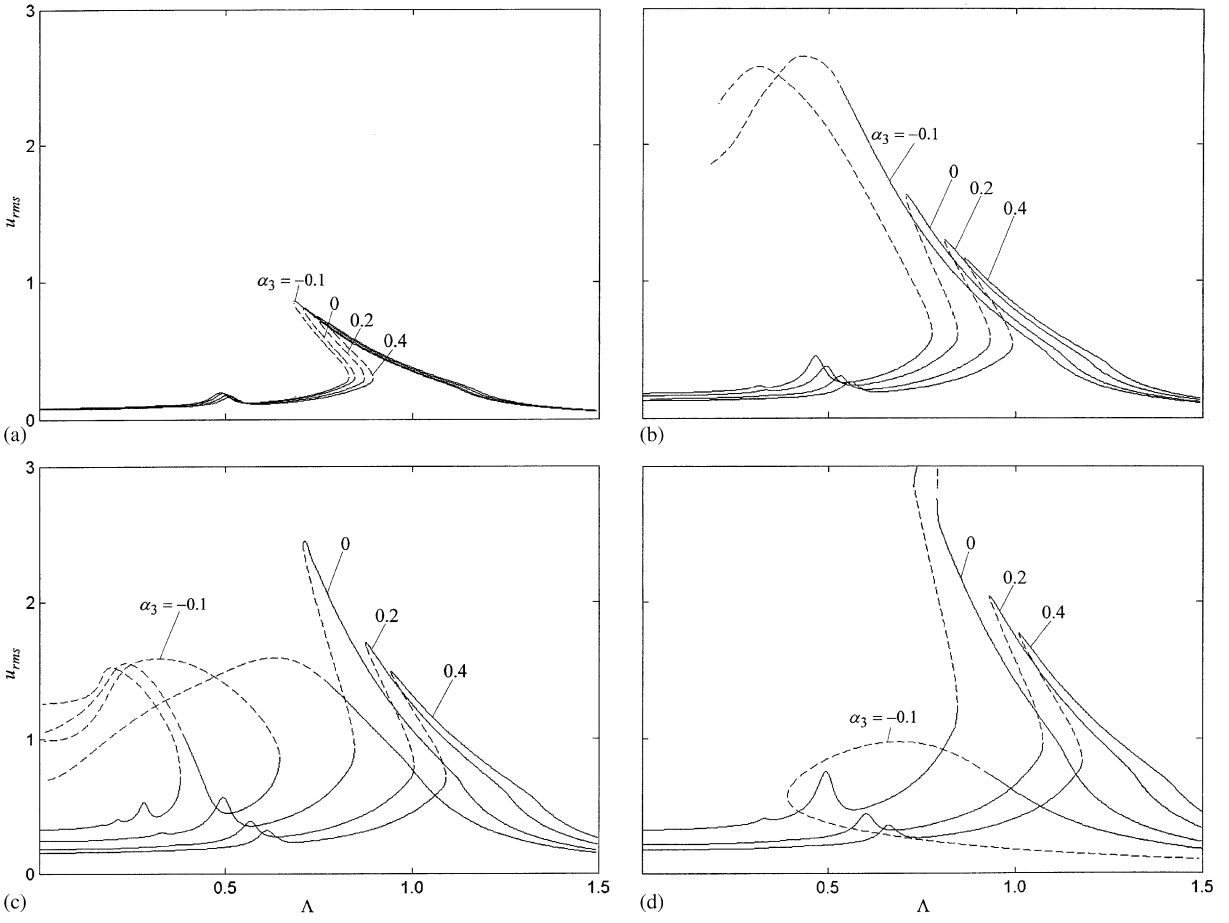


Fig. 3. $u_{\mathrm{rms}}$ of an oscillator with $\alpha_1 = 1$, $\alpha_2 = 0$ and $\alpha_3 = -0.1$, 0.0, 0.2 and 0.4, given $f_i = 0$ $(i \geqslant 2)$, $w_3 = 0.3$, $\zeta = 0.05$ for (a) $f_1 = 0.25$, (b) $f_1 = 0.5$, (c) $f_1 = 0.75$, and (d) $f_1 = 1.0$. (—) stable and (– –) unstable HBM solutions.

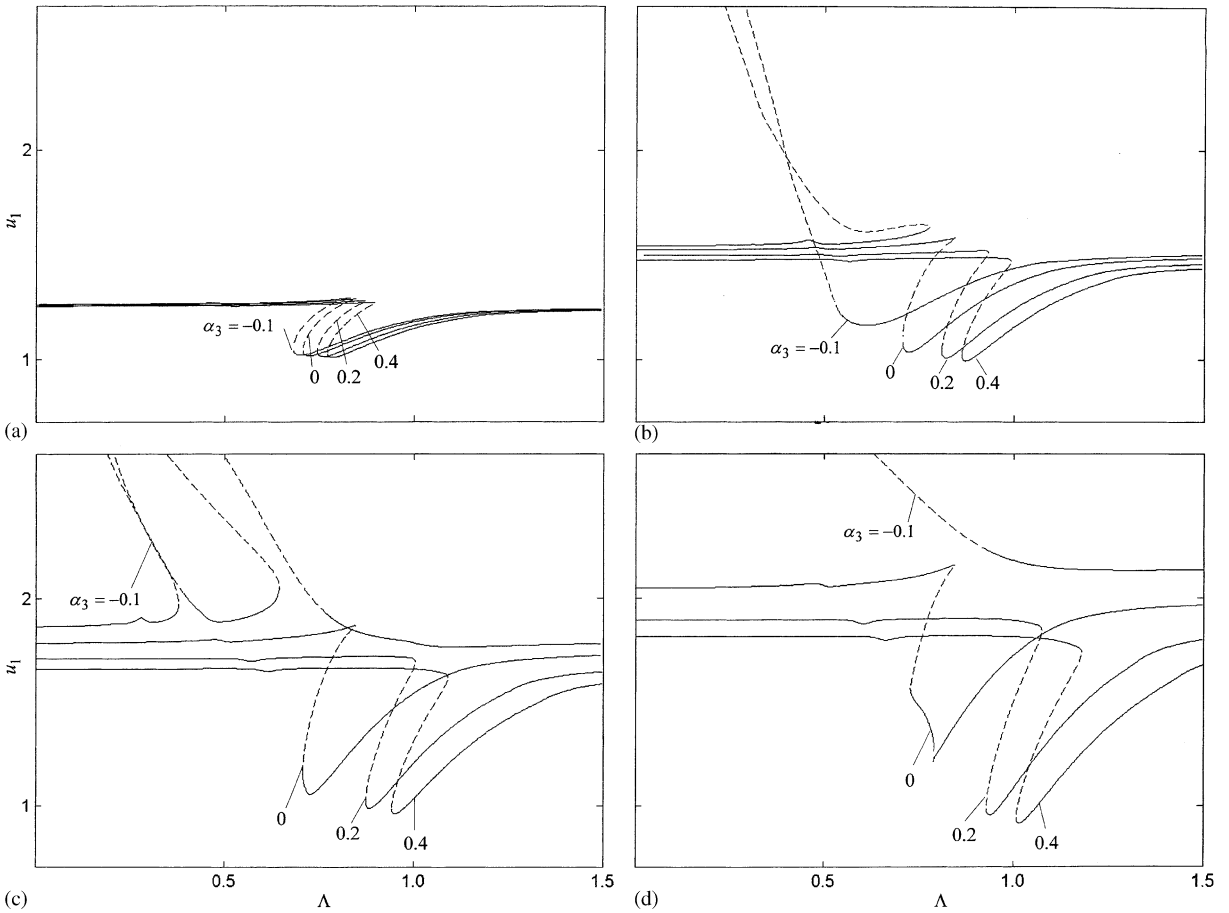


Fig. 4. $u_1$ of the same oscillator as that in Fig. 3: (a) $f_1 = 0.25$, (b) $f_1 = 0.5$, (c) $f_1 = 0.75$, and (d) $f_1 = 1.0$. (—) stable and (– –) unstable HBM solutions.

corresponding to the primary resonance due to internal harmonic excitation $w_3$. Additionally, the responses for $\alpha_3 \neq 0$ and $\alpha_3 = 0$ are quite close because of the fact that the vibrations take place in a portion of $g[u(\tau)]$ where the cubic nonlinearity is not significant enough. For instance, at $\Lambda = 1$ where $u_1 \approx 1.15$ and $u_{\text{rms}} \approx 0.35$, $u(\tau)$ varies roughly between 0.8 and 1.5, and $g[u(\tau)]$ is nearly linear within this range. However, with the increasing of $f_1$, the value of $u_1$ is enlarged as well, which moves the range of $u(\tau)$ to the right in Fig. 1, where cubic nonlinearity becomes more important. Thus, the behavior of the oscillator is changed significantly as shown in Figs. 3(b) and 4(b), which have the same parameters as those of Figs. 3(a) and 4(a), except $f_1 = 0.50$.

The effect of $\alpha_3$ in Figs. 3 and 4 is such that a positive $\alpha_3$ (hardening) shifts the response to the right and reduces the vibration amplitudes slightly while the overall shape of the motion remains similar to the case of $\alpha_3 = 0$. Meanwhile, a negative $\alpha_3$ (softening) causes the primary resonance peak to shift to the left, and the vibration amplitudes may increase significantly on the upper branch before a jump-down takes place. In Figs. 3(c,d) and 4(c,d) for $f_1 = 0.75$ and 1.0,

respectively, the same effect of a hardening $\alpha_3$ is observed except the changes in resonance frequencies and vibration amplitudes become more severe. The response for $\alpha_3 = -0.1$ differs drastically. In Fig. 3(c), the primary resonance peak is at nearly $\Lambda = 0.8$, and the upper branch solution loses its stability at about $\Lambda = 0.7$. There is no stable period-1 motion for $\Lambda \in [0.63, 0.7]$, in which stable subharmonic motions exist [48]. The superharmonic resonance peak (at half the primary resonance frequency) becomes larger, and exhibits an SSI solution. Finally, when $f_1 = 1.0$ in Figs. 3(d) and 4(d), the PL system for $\alpha_3 = 0$ displays DSI motions at the end of the SSI branch. These DSI motions are eliminated for $\alpha_3 > 0$. For $\alpha_3 = -0.1$, there is no stable period-1 motion for $\Lambda < 0.82$. In summary, the behavior displayed in Figs. 3 and 4 indicates that the impact of cubic nonlinearity depends heavily on the value of the preload. A larger $f_1$ makes the influence of $\alpha_3$ more significant. On the contrary, a PL approximation for $g[u(\tau)]$ might be sufficient when $f_1$ is small regardless of $\Lambda$.

The effect of damping ratio is illustrated in Fig. 5 for the same parameters as in Fig. 3 except $w_3 = 0.3$, and $\zeta = 0.025$, 0.05, 0.075, and 0.1. As expected, a lower $\zeta$ value results in larger $u_{\text{rms}}$

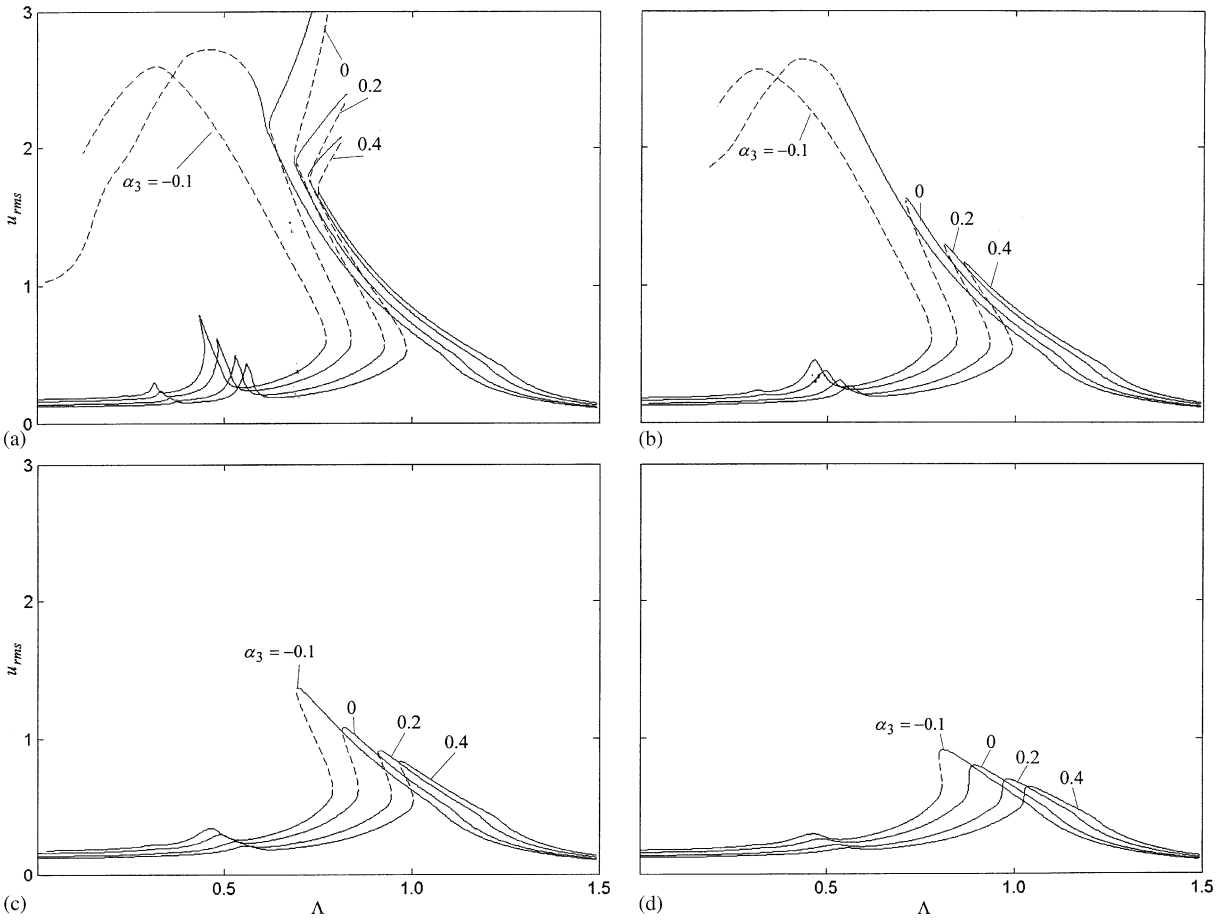


Fig. 5. $u_{\text{rms}}$ of an oscillator with $\alpha_1 = 1$, $\alpha_2 = 0$ and $\alpha_3 = -0.1$, 0.0, 0.2 and 0.4, given $f_i = 0$ $(i \geqslant 2)$, $f_1 = 0.5$, $w_3 = 0.3$ for (a) $\zeta = 0.025$, (b) $\zeta = 0.05$, (c) $\zeta = 0.075$, and (d) $\zeta = 0.1$ (—). stable and (– –) unstable HBM solutions.

amplitudes as well as several types of nonlinear behaviors including SSI and DSI motions and superharmonic resonances. For instance, in Fig. 5(a) for $\zeta = 0.025$, all response curves for $\alpha_3 \geqslant 0$ show hardening-type DSI motions at the end of large-amplitude softening-type SSI motions. For $\alpha_3 = -0.1$, on the other hand, DSI motions do not exist while the SSI motions have even higher amplitudes. Further increasing the value of $\zeta$, first DSI motions are eliminated, and then the SSI amplitudes are reduced significantly. For instance, motions are mostly NI type for $\zeta = 0.1$ as shown in Fig. 5(d).

Fig. 6 demonstrates the combined influence of $\alpha_3$ and $w(\tau)$ on $u_{\text{rms}}$, where $\alpha_1 = 1$, $\alpha_2 = 0$ and $\alpha_3 = -0.1, 0, 0.2$ and 0.4, $\zeta = 0.05$, $f_1 = 0.5$, and all other $f_i = 0$. The stiffness function $w(\tau)$ is considered to be harmonic with amplitude $w_3 = 0.1$, 0.2, 0.3 and 0.4. Fig. 6 indicates that the magnitude of $u_{\text{rms}}$ gets larger when $w_3$ is increased. When $w_3 = 0.1$, all response curves are approximately linear with no impacts as shown in Fig. 6(a). This agrees with previous studies on PL systems, which stated that separations could not occur if $w_3 \leqslant 2\zeta$ [31,32]. When $w_3 = 0.2$, softening-type nonlinear curves from SSI motions are introduced. Increasing $\alpha_3$ reduces the

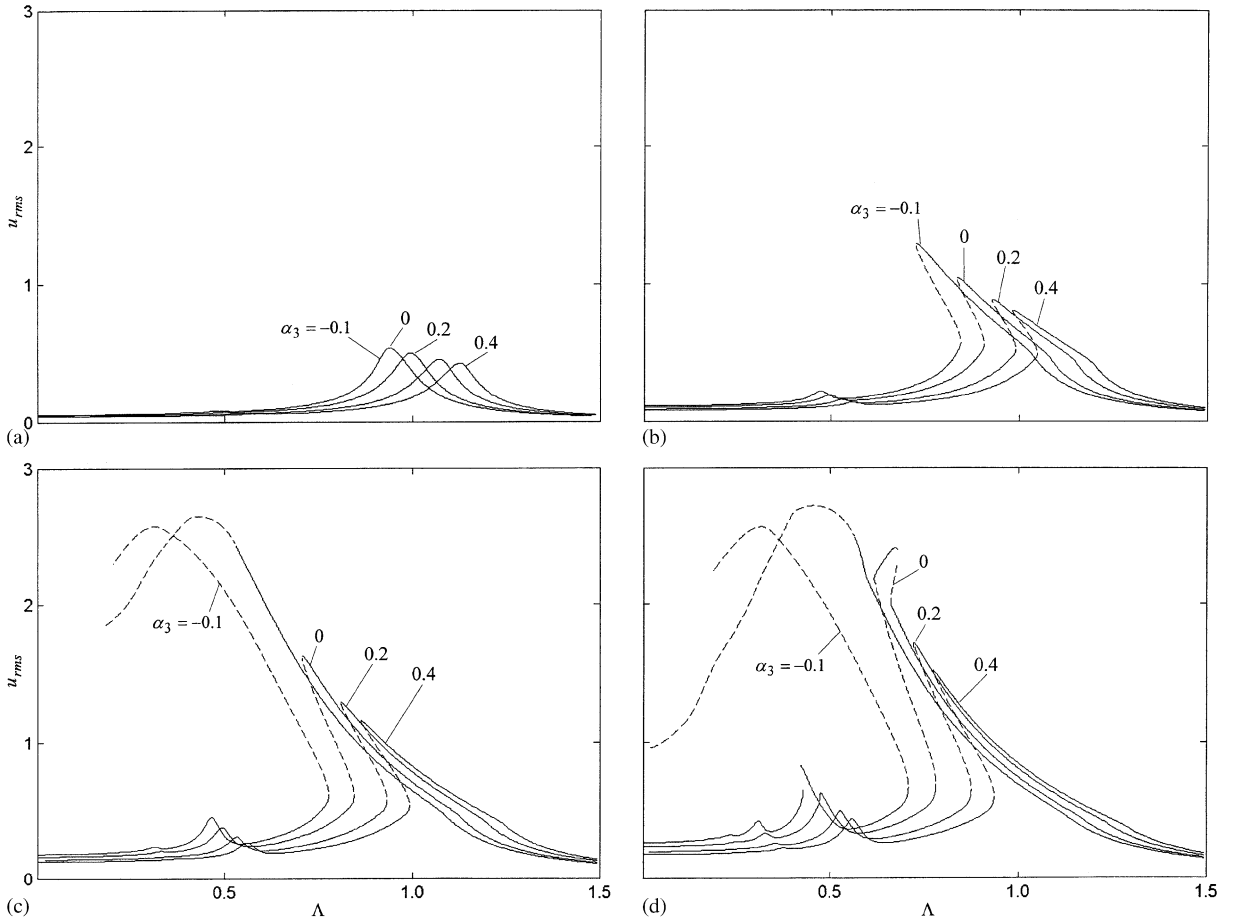


Fig. 6. $u_{\text{rms}}$ of an oscillator with $\alpha_1 = 1$, $\alpha_2 = 0$ and $\alpha_3 = -0.1$, 0.0, 0.2 and 0.4, given $f_i = 0$ $(i \geqslant 2)$, $f_1 = 0.5$, $\zeta = 0.05$ for (a) $w_3 = 0.1$, (b) $w_3 = 0.2$, (c) $w_3 = 0.3$, and (d) $w_3 = 0.4$. (—) stable and (– –) unstable HBM solutions.

amplitude of vibrations, and moves the resonance peaks to higher frequencies. This is also true with larger $w_3$ values as in Figs. 6(c,d) for $w_3 = 0.3$ and 0.4, respectively. When $w_3 = 0.4$, the PL system ($\alpha_3 = 0$) exhibits DSI motions, which are eliminated when $\alpha_3 = 0.2$ and 0.4. DSI motions do not exist for $\alpha_3 = -0.1$ either, and the amplitude of the superharmonic resonance (at half the frequency of the primary resonance) peak is quite large with a slight separation.

In Fig. 7, a harmonic external excitation is considered without any stiffness fluctuations ($w(\tau) = 1$). The system parameters are kept the same as in Fig. 6 except $\zeta = 0.05$ and $f_3 = 0.05$, 0.1, 0.2 and 0.3. For $\alpha_3 = 0$, a good agreement with previous studies on PLTI system [26] is obtained, in the sense that increasing $f_3$ enlarges the amplitudes in the vicinity of the primary resonance. In Fig. 7(b), both SSI and DSI motions are presented for $f_3 = 0.1$. When the ratio of $f_3/f_1$ is small, say $f_3/f_1 < 0.5$, no significant superharmonic resonances are evident in Fig. 7, especially for the PL system, unlike Fig. 6 for $w(\tau) \neq 0$. However, when $f_3/f_1$ is large enough ($f_3/f_1 = 0.6$ in Fig. 7(d)), superharmonic resonance amplitudes are increased significantly. This suggests that not only the individual values of $f_1$ and $f_3$, but also their ratio $f_3/f_1$, are critical. For

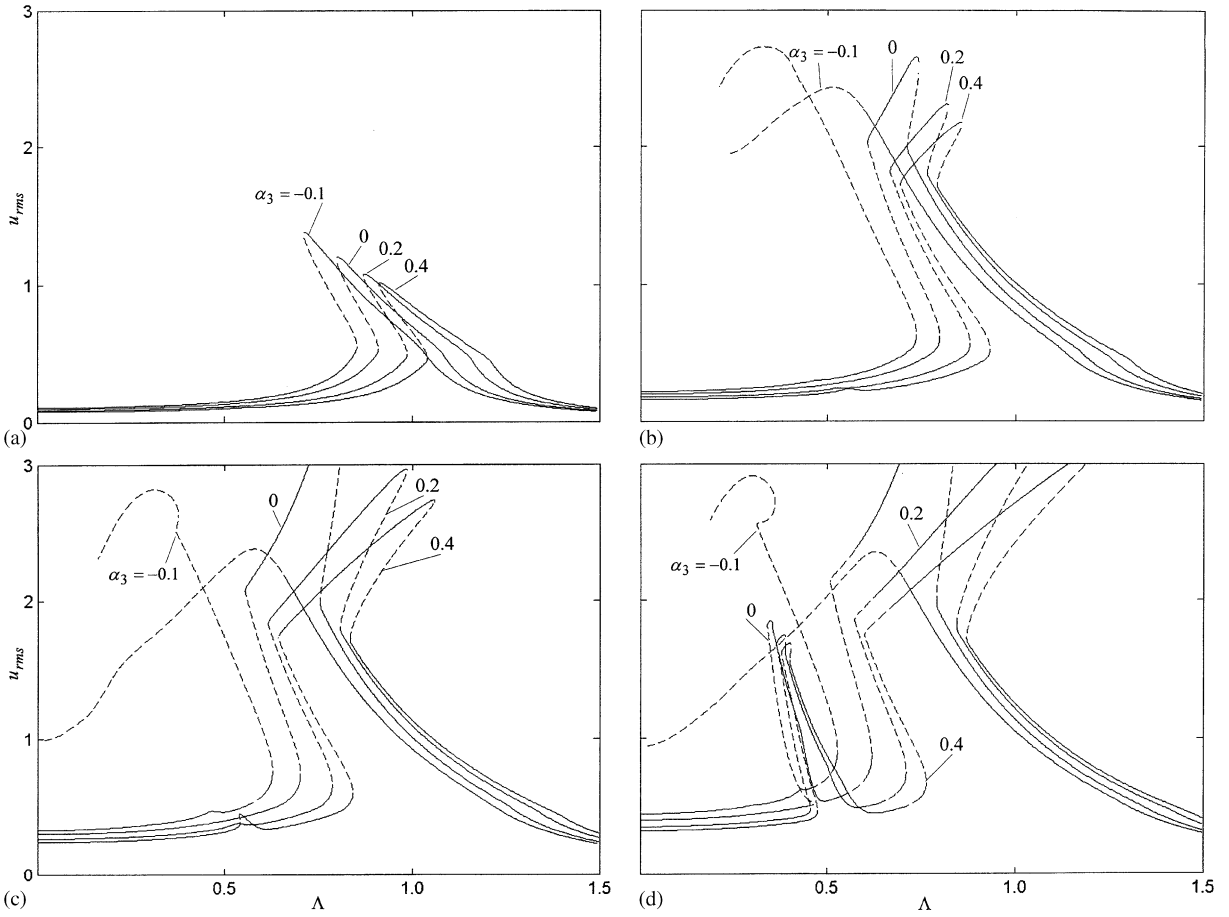


Fig. 7. $u_{\mathrm{rms}}$ of an oscillator with $\alpha_1 = 1$, $\alpha_2 = 0$ and $\alpha_3 = -0.1$, 0.0, 0.2 and 0.4, given $w_i = 0$ ($i \geqslant 2$), $f_1 = 0.5$, $\zeta = 0.05$ for (a) $f_3 = 0.05$, (b) $f_3 = 0.1$, (c) $f_3 = 0.2$, and (d) $f_3 = 0.3$. (—) stable and (– –) unstable HBM solutions.

different values of $f_1$ and $f_3$, having the same ratio $f_3/f_1$, the response curves maintain the same qualitative shape and primary resonances. The influence of $\alpha_3$ is the same as before.

In Fig. 8, harmonic internal and external excitations, $w(\tau)$ and $f(\tau)$, are applied simultaneously. Here $\kappa = \mu = 1$, and $w(\tau)$ and $f(\tau)$ are in-phase. This is accomplished by considering $f_3$ and $w_3$ only in Eq. (3). With $w_3 = 0.3$ kept constant, $f_3$ is varied from 0.01 to 0.2 in Fig. 8. For a very small $f_3$, the nonlinear response in Fig. 8(a) is primarily due to $w_3$, which can be confirmed by a comparison with Fig. 6(c). As the value of $f_3$ is increased, the amplitude of response decreases first as shown in Figs. 8(b) and (c) to a point that there are only NI motions in Fig. 8(c) for $f_3 = 0.1$. However, $u_{\text{rms}}$ increases and softening-type SSI response reappears in Fig. 8(d) for $f_3 = 0.2$. This suggests that $w(\tau)$ and $f(\tau)$ tend to cancel each other when they are in-phase. It can also be shown for in-phase harmonic excitations that $u_{\text{rms}} = 0$ and $u_1$ is a constant when $w_i = f_i/f_1$ $(i \geqslant 2)$ regardless of the value of $\alpha_i$.

An 180° out-of-phase condition is accomplished in Fig. 9 by simply setting $w_3 = 0.3$ and $f_3 = -0.01$, –0.05, –0.1 and –0.2. Here two excitations act in such a way that their effects on

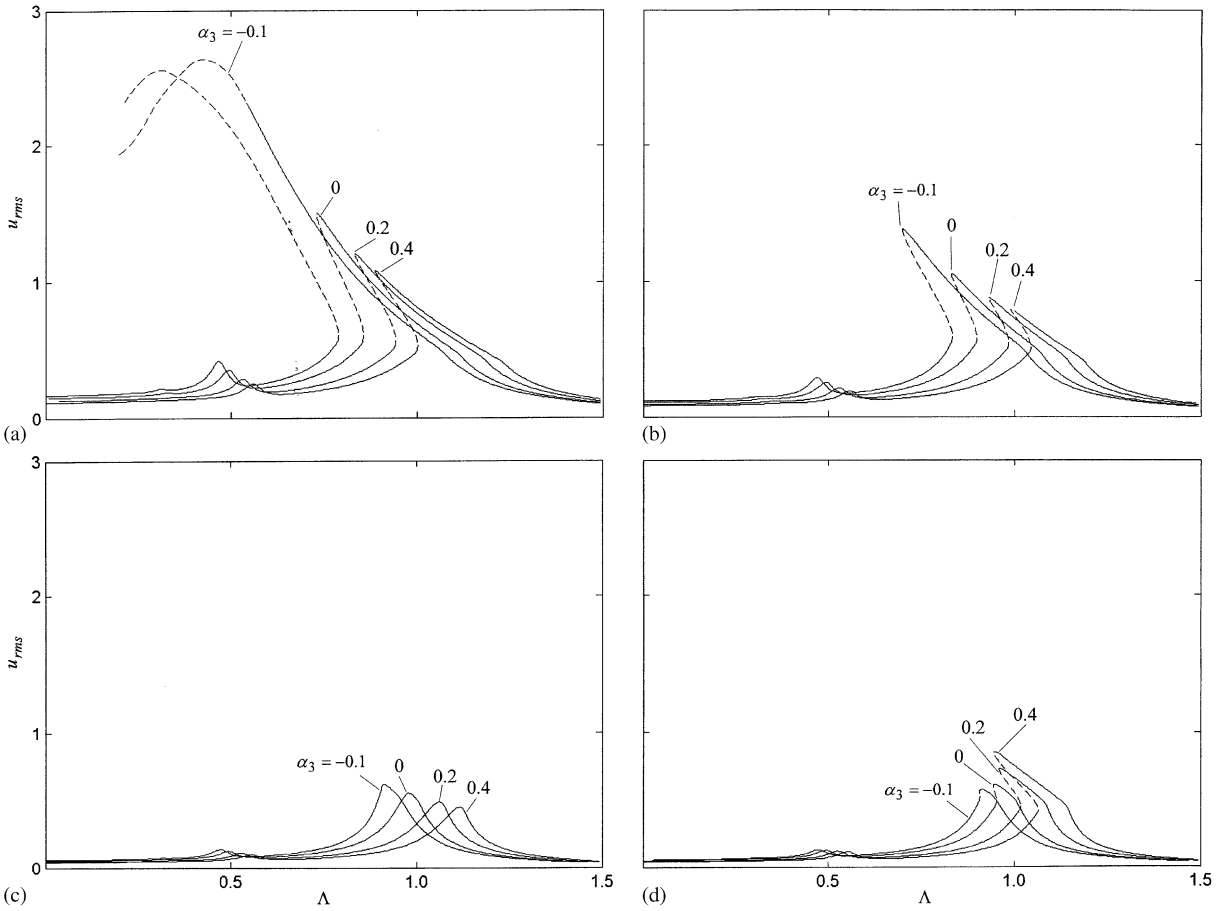


Fig. 8. $u_{\text{rms}}$ of an oscillator with $\alpha_1 = 1$, $\alpha_2 = 0$ and $\alpha_3 = -0.1, 0.0, 0.2$ and 0.4, given $w_3 = 0.3, f_1 = 0.5, \zeta = 0.05$ for (a) $f_3 = 0.01$, (b) $f_3 = 0.05$, (c) $f_3 = 0.1$, and (d) $f_3 = 0.2$. (—) stable and (– –) unstable HBM solutions.

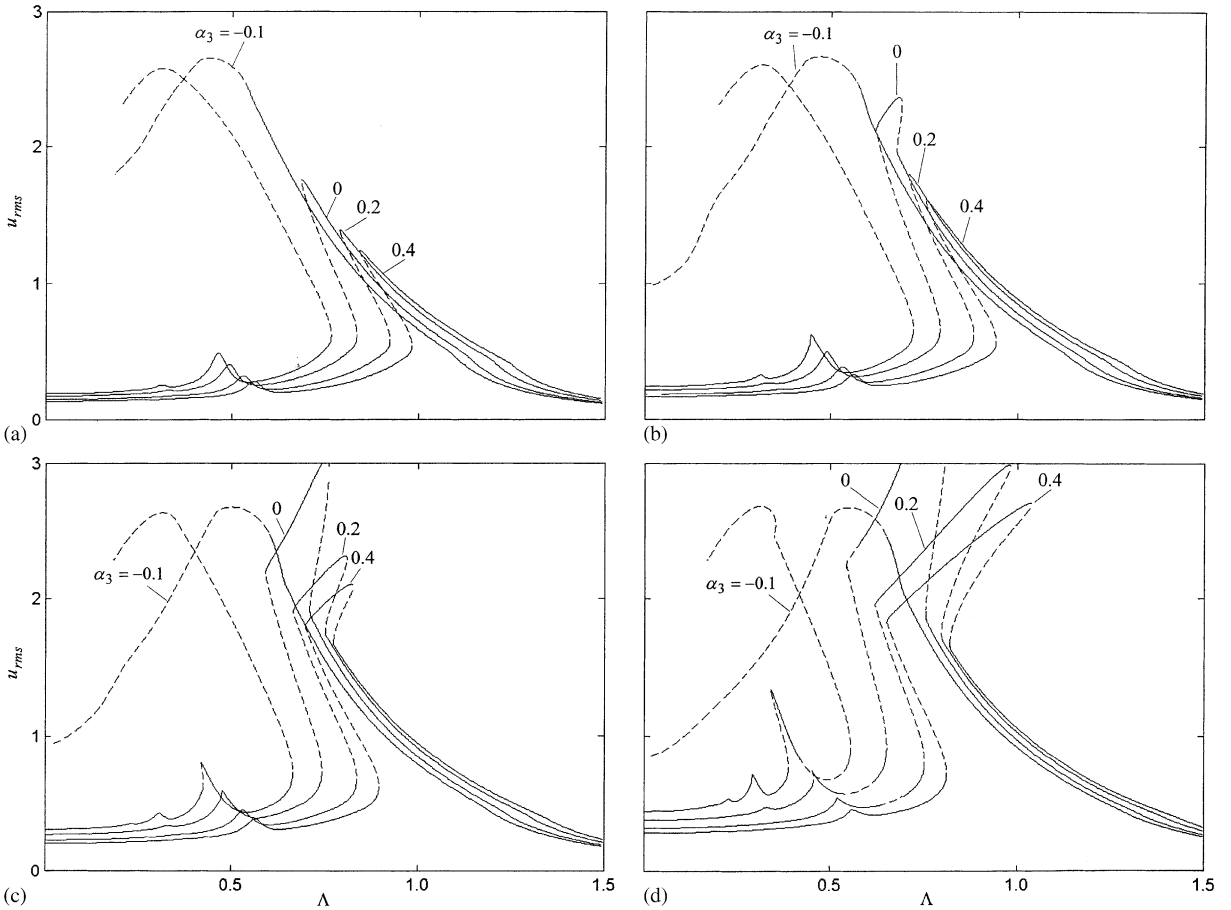


Fig. 9. $u_{\text{rms}}$ of an oscillator with $\alpha_1 = 1$, $\alpha_2 = 0$ and $\alpha_3 = -0.1, 0.0, 0.2$ and 0.4, given $w_3 = 0.3, f_1 = 0.5, \zeta = 0.05$ for (a) $f_3 = -0.01$, (b) $f_3 = -0.05$, (c) $f_3 = -0.1$, and (d) $f_3 = -0.2$. (—) stable and (– –) unstable HBM solutions.

system response add to each other. In contrast to Fig. 8, response amplitudes are enlarged significantly with increasing $f_3$. Very large DSI motions are observed in Fig. 9(d) for $w_3 = 0.3$ and $f_3 = -0.2$ when $\alpha_3 \geqslant 0$, and large superharmonic resonance peaks are obtained when $\alpha_3 = -0.1$. A similar dependence of the response on the phasing relationship between $w(\tau)$ and $f(\tau)$ was reported earlier for PL systems as well [31,32].

Next, consider the case when $2\kappa = \mu$ as shown in Fig. 10. Here, all parameters except $w_i$ and $f_i$ ($i \geqslant 2$) are the same as those in Fig. 9. The value of $w_3$ is kept constant at 0.3, and $f_5$ is varied from 0.01 to 0.2. In Fig. 10(a), the nonlinear response is mainly due to $w_3$ since the value of $f_5$ is relatively small. $w_{2\kappa+1} = w_3$ results in a primary resonance near $\Lambda = 1/\kappa = 1$ and a superharmonic resonance near $\Lambda = 1/(2\kappa) = \frac{1}{2}$. Examining Figs. 10(a–d), one concludes that the response near $\Lambda = 1$ remains almost the same for different $\alpha_3$, respectively, since $w_3$ is kept constant, confirming that $f_5$ has a negligible effect near $\Lambda = 1$. Increasing the value of $f_{2\mu+1} = f_5$, the response near $\Lambda = 1/\mu = \frac{1}{2}$ is amplified. SSI motions appear in Fig. 10(b) for $f_5 = 0.05$, and DSI motions appear in Fig. 10(d) for $f_5 = 0.2$. The effects of $w(\tau)$ and $f(\tau)$ are superimposed in

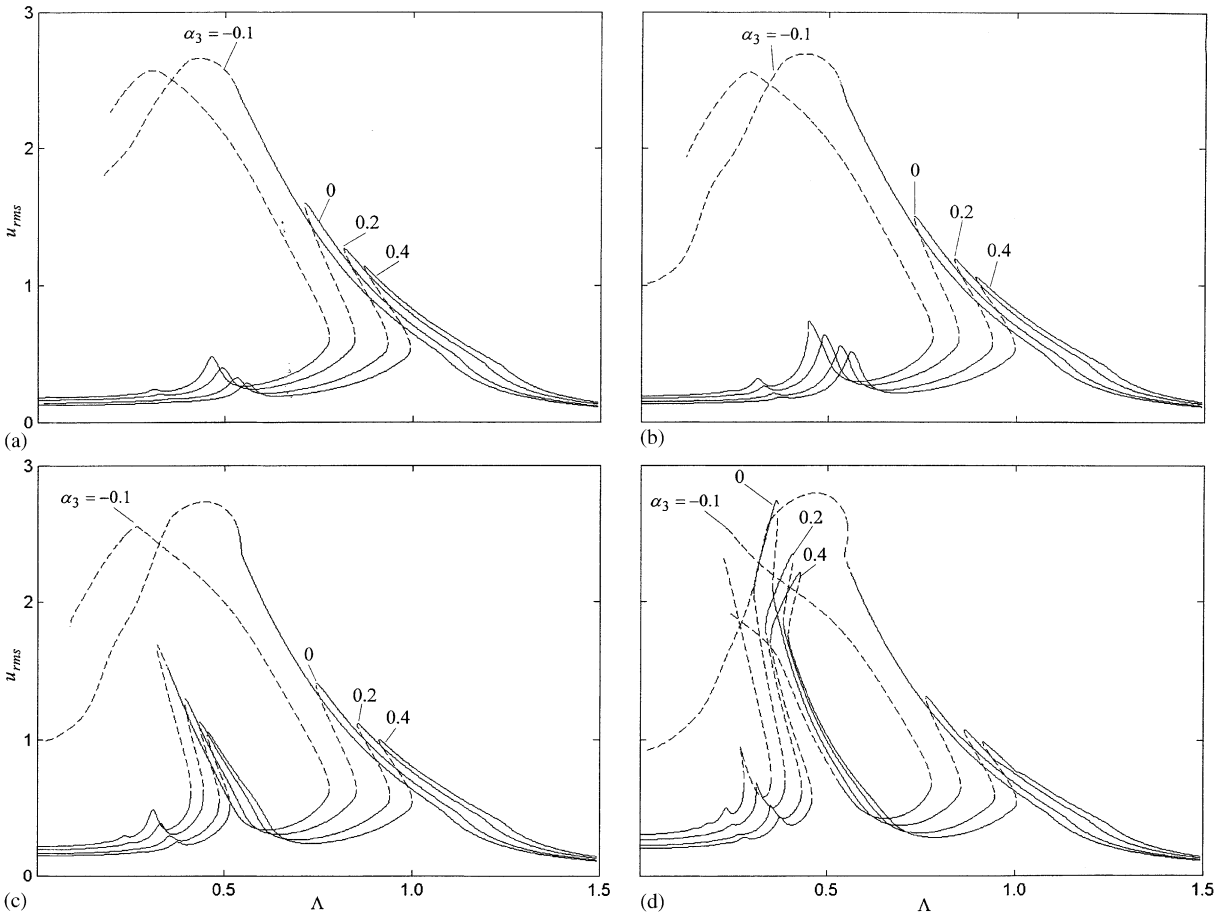


Fig. 10. $u_{\text{rms}}$ of an oscillator with $\alpha_1 = 1$, $\alpha_2 = 0$ and $\alpha_3 = -0.1, 0.0, 0.2$ and 0.4, given $w_3 = 0.3, f_1 = 0.5, \zeta = 0.05$ for (a) $f_5 = 0.01$, (b) $f_5 = 0.05$, (c) $f_5 = 0.1$, and (d) $f_5 = 0.2$. (—) stable and (– –) unstable HBM solutions.

terms of primary resonances, and superharmonic activity at $\Lambda = 1/(3\kappa) = \frac{1}{3}$ is increased significantly. The effect of increasing $\alpha_3$ is the same as before, in terms of decreased $u_{\text{rms}}$ and increased primary resonance frequencies.

Fig. 11 represents the response when $\kappa = 2\mu$ with all parameters the same as in Fig. 11. In this figure, $f_3 = 0.05$ and $w_5 = 0.1$, 0.2, 0.3 and 0.4. In line with Figs. 6(a) and 7(a), Fig. 11(a) has a resonance peak near $\Lambda = 1/\mu = 1$ due to $f_{2\mu+1} = f_3$, and another peak at $\Lambda = 1/\kappa = \frac{1}{2}$ due to $w_{2\kappa+1} = w_5$. The value of $w_5 = 0.1$ is not large enough to either cause SSI motions near $\Lambda = 1/\kappa = \frac{1}{2}$ or a parametric resonance near $\Lambda = 2/\kappa = 1$. As a result, the activity near $\Lambda = 1$ can mostly be attributed to $f_3$. For the rest of the cases in Figs. 11(b–d), a larger $w_5$ has a greater influence on the vibration amplitudes around $\Lambda = 1$. DSI motions appear when $w_5 \geqslant 0.2$, and the $u_{\text{rms}}$ values increase drastically in Figs. 11(c,d) near $\Lambda = 1$. This is because the parametric resonance due to $w_5$ and the primary resonance due to $f_3$ act near the same frequency of $\Lambda = 2/\kappa = 1/\mu = 1$. Meanwhile, in Fig. 11(d) for $w_5 = 0.4$ superharmonic resonances are created at $\Lambda = 1/(2\kappa) = \frac{1}{4}$ and $1/(3\kappa) = \frac{1}{6}$ as well.

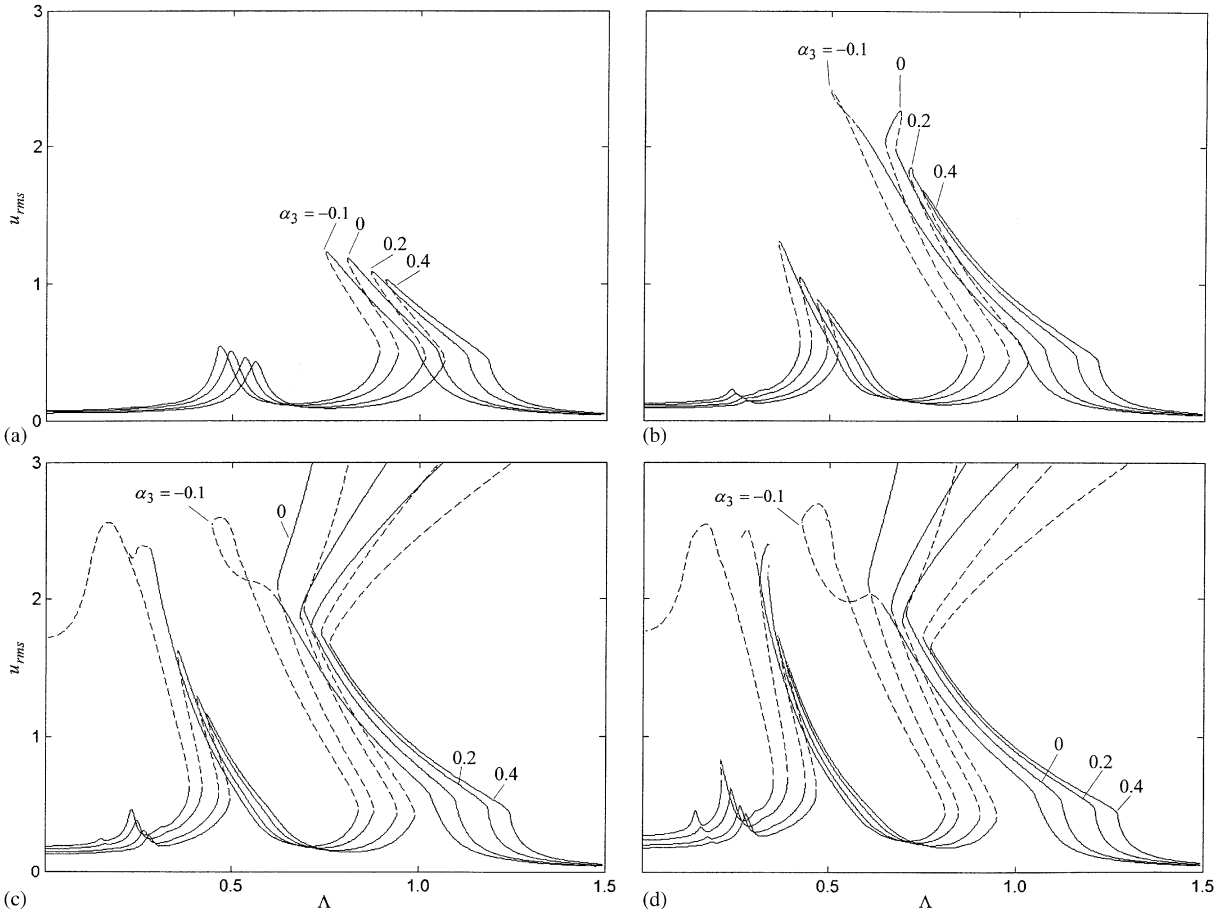


Fig. 11. $u_{\mathrm{rms}}$ of an oscillator with $\alpha_1 = 1$, $\alpha_2 = 0$ and $\alpha_3 = -0.1$, 0.0, 0.2 and 0.4, given $w_3 = 0.3$, $f_1 = 0.5$, $\zeta = 0.05$ for (a) $w_5 = 0.1$, (b) $w_5 = 0.2$, (c) $w_5 = 0.3$, and (d) $w_5 = 0.4$. (—) stable and (– –) unstable HBM solutions.

### 3.2. $\alpha_1 = 1$, $\alpha_3 = 0$, *and variable* $\alpha_2$

In this case, $g[u(\tau)]$ is defined by a constant linear term $\alpha_1 = 1$ and a quadratic nonlinear term $\alpha_2$ with no cubic term ($\alpha_3 = 0$). The value of $\alpha_2$ is varied between –0.1 and 0.4 including $\alpha_2 = 0$. All of the parametric studies presented in Section 3.1 were carried out for the case of quadratic nonlinearities as well. As the influence of $\alpha_2$ is quite similar to $\alpha_3$, at least qualitatively, only a representative example is shown here in Fig. 13. This figure presents the combined effect of $f_1$ and $\alpha_2$ on the response.

By comparing Figs. 3 and 12, several differences can be noted. (1) For softening cases ($\alpha_2 = -0.1$ versus $\alpha_3 = -0.1$), the responses are quite different. The response curves for $\alpha_2 = -0.1$ are much like extensions of those of the PL system in contrast to the erratic and mostly unstable behavior for $\alpha_3 = -0.1$. (2) For the hardening cases, the results for $\alpha_2 = 0.2$ and 0.4 are quite similar to corresponding cases in Fig. 4 for $\alpha_3 = 0.2$ and 0.4 except the amplitudes increase slightly. The changes near $\Lambda = 1$ with $\alpha_2$ are not as significant as the corresponding changes

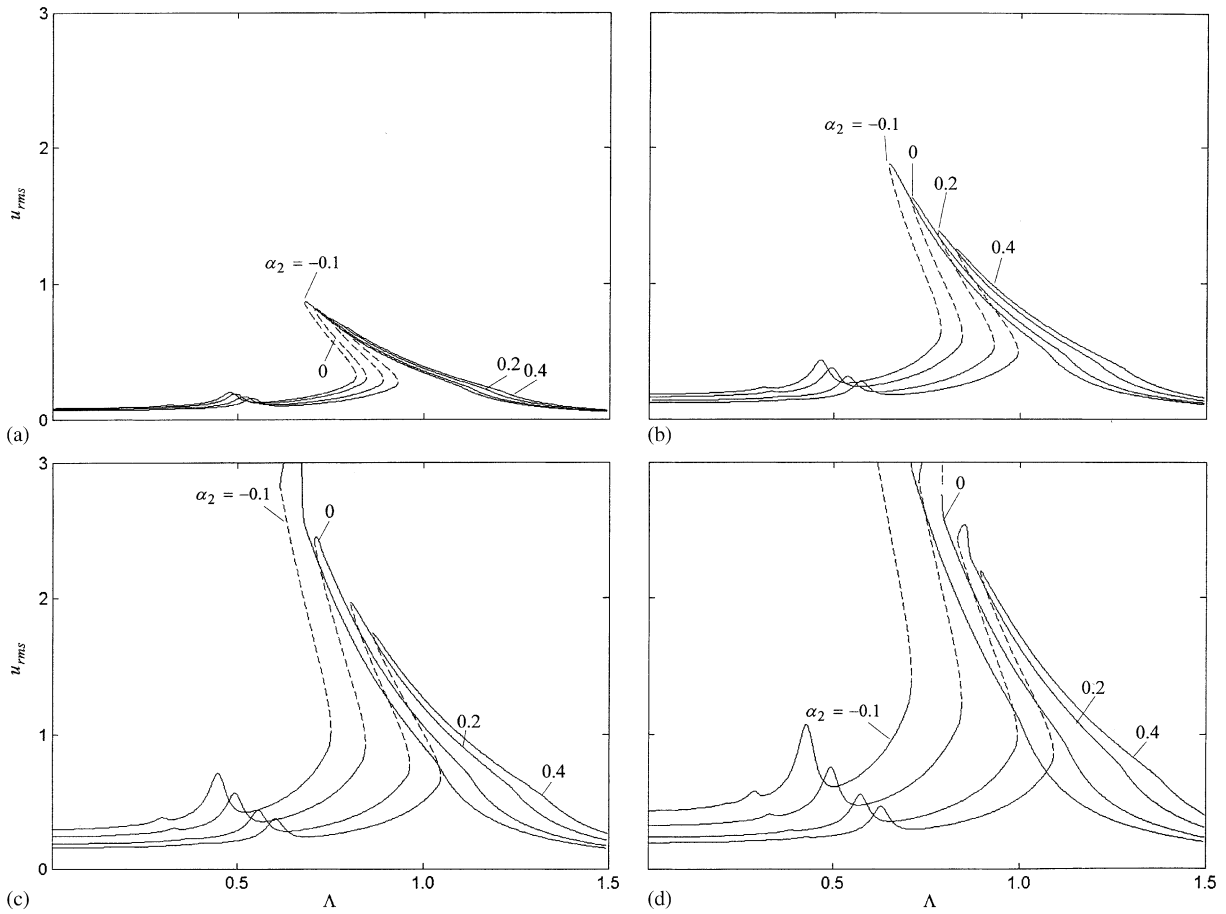


Fig. 12. $u_{\text{rms}}$ of an oscillator with $\alpha_1 = 1$, $\alpha_2 = -0.1$, 0.0, 0.2 and 0.4 and $\alpha_3 = 0$, given $f_i = 0$ $(i \geqslant 2)$, $w_3 = 0.3$, $\zeta = 0.05$ for (a) $f_1 = 0.25$, (b) $f_1 = 0.5$, (c) $f_1 = 0.75$, and (d) $f_1 = 1.0$. (—) stable and (– –) unstable HBM solutions.

with $\alpha_3$ in Fig. 3. This suggests that the effect of $\alpha_2$ on system response is not as significant as that of $\alpha_3$ having the same values. (3) DSI motions are predicted for $\alpha_2 = -0.1$ in Figs. 12(c,d), while no DSI motions are evident in Fig. 3 for $\alpha_3 = -0.1$.

### 3.3. $\alpha_1 = 1$ *and variable* $\alpha_2$ *and* $\alpha_3$

As the final case, both quadratic and cubic nonlinearities are considered simultaneously. Four sets of parameters are used: (1) $\alpha_2 = \alpha_3 = -0.1$, (2) $\alpha_2 = -0.1$, $\alpha_3 = 0.2$, (3) $\alpha_2 = 0.2$, $\alpha_3 = -0.1$, and (4) $\alpha_2 = \alpha_3 = 0.2$. In Fig. 13, the response curves for these four cases are compared for different $f_1$ values. The corresponding restoring functions $g[u(\tau)]$ are plotted schematically in the upper right corner for each case to demonstrate the shape of $g[u(\tau)]$. In Fig. 13(a), both nonlinearities are of the softening type, which makes the system response very dramatic and quite unstable. No stable period-1 solutions could be found for $f_1 = 1.0$ within this frequency range for

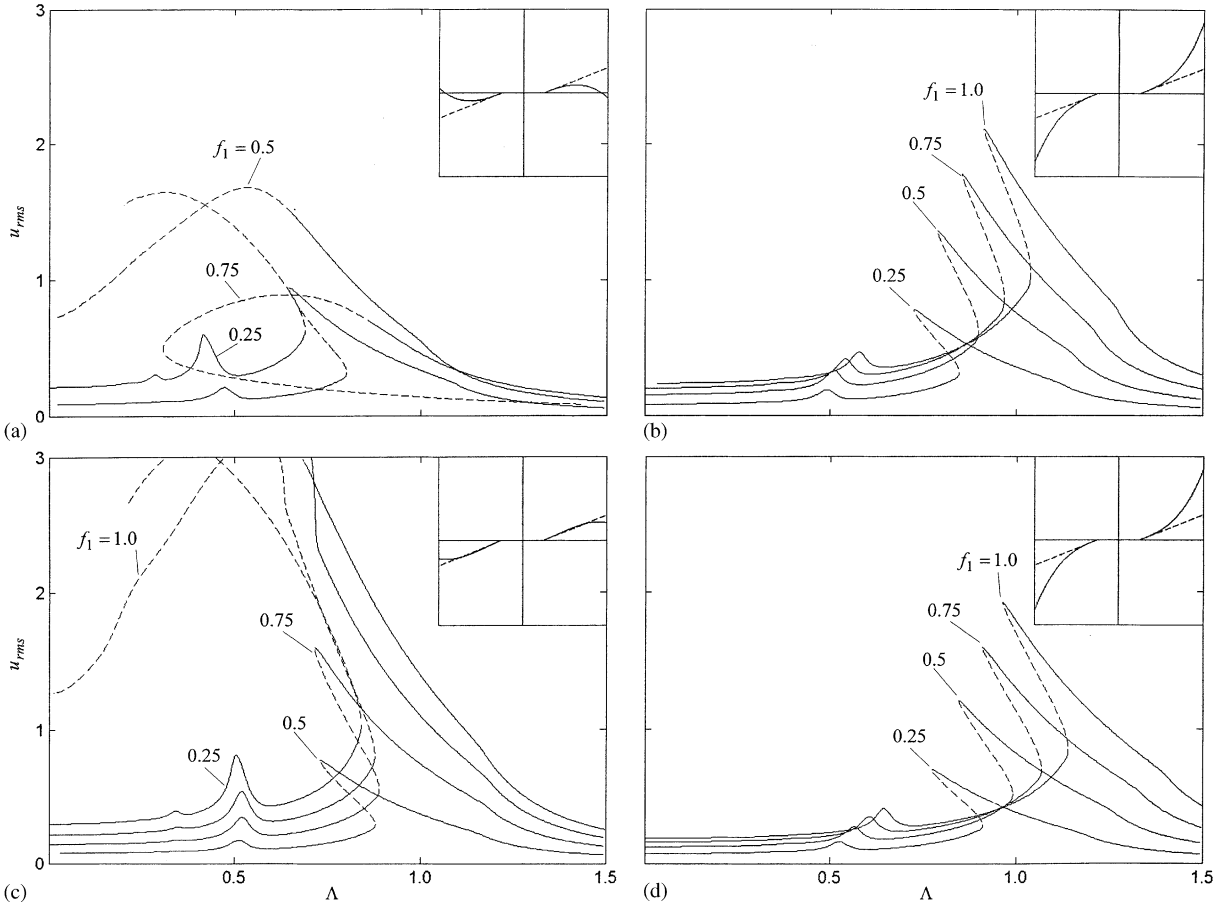


Fig. 13. $u_{\text{rms}}$ of an oscillator with $\alpha_1 = 1$, variable $\alpha_2$ and $\alpha_3$, given $f_i = 0$ $(i \geqslant 2)$, $w_3 = 0.3$, $\zeta = 0.05$, $f_1 = 0.25, 0.5, 0.75$ and 1.0 for (a) $\alpha_2 = \alpha_3 = -0.1$, (b) $\alpha_2 = -0.1$, $\alpha_3 = 0.2$, (c) $\alpha_2 = 0.2$, $\alpha_3 = -0.1$, and (d) $\alpha_2 = \alpha_3 = 0.2$. (—) stable and (– –) unstable HBM solutions.

this case. However, if the signs of $\alpha_2$ and $\alpha_3$ are opposite, they tend to cancel each other. In Fig. 13(c), the response curves are very similar to the results of the corresponding PL system, and the amplitudes near primary and superharmonic resonances are similar to those of the PL system for each $f_1$ value considered. In addition, $\alpha_3$ has a more dominant effect on system response than $\alpha_2$. This can be confirmed by comparing the results in Figs. 13(b,d).

## 4. Conclusions

In this study, the dynamic behavior of a piecewise-nonlinear oscillator subjected to a preload and combined parametric and external excitations was considered. The oscillator has a time-varying stiffness as well as a restoring function formed by clearance and continuous nonlinearities. Analytical solutions were obtained by employing the multi-term HBM in conjunction with the

Newton–Raphson method, DFT, and the generic homotopy method. The stability of steady-state response was determined by applying Floquet theory. The HBM solutions were verified by comparing them to the direct numerical integration results. In addition, DFM was used to derive single-term harmonic balance solutions for the same system. Several key characteristics of the system were demonstrated through a detailed parametric study. Among these characteristics, the effects of continuous nonlinearities are very sensitive to the value of mean load $f_1$. Both quadratic and cubic nonlinearities are more influential for larger $f_1$ values. As a general trend, the amplitudes of $u_{\text{rms}}$ near the primary resonance peaks are decreased, and the resonance peaks are shifted to high frequencies with increases of the values of $\alpha_2$ and $\alpha_3$. In the presence of a parametric excitation of harmonic order $\kappa$, a primary resonance at $\Lambda = 1/\kappa$ is obtained as well as a sizable superharmonic resonance at $\Lambda = 1/(2\kappa)$. For a case of external excitation $f(\tau)$ only, superharmonic resonances appear only when the ratio of alternating component to mean load $f_i/f_1$ is quite large. When both internal and external excitations act simultaneously, they appear to cancel each other when two excitations are in phase and of the same fundamental frequency, and add to each other when they are 180° out of phase. Moreover, when $w_i = f_i/f_1$, $u_{\text{rms}} = 0$, and $u_1$ remains constant regardless of the values of $\alpha_2$, $\alpha_3$ and $\Lambda$. While both SSI and DSI motions are predicted for $\alpha_2 \geqslant 0$ and $\alpha_3 \geqslant 0$, DSI motions are not common for $\alpha_{3<}0$. Finally, the overall impact of quadratic nonlinearity on the system response seems to be less significant than that of a cubic nonlinearity.

## References

[1] A. Kahraman, A spline joint formulation for drive train torsional dynamic models, *Journal of Sound and Vibration* 241 (2) (2001) 328–336.
[2] P.R. Nayak, Contact vibrations, *Journal of Sound and Vibration* 22 (3) (1972) 297–322.
[3] J. Sabot, P. Krempf, C. Janolin, Nonlinear vibrations of a sphere–plane contact excited by a normal load, *Journal of Sound and Vibration* 214 (2) (1998) 359–375.
[4] E. Rigaud, J. Perret-Liaudet, Experiments and numerical results on nonlinear vibrations of an impacting Hertzian contact. Part 1: harmonic excitation, *Journal of Sound and Vibration* 265 (2) (2003) 289–307.
[5] J. Perret-Liaudet, Résonance sous-harmonique d'ordre deux dans un contact sphère-plan, *Comptes Rendus de l'Académie des Sciences* 325 (Série II-b) (1997) 443–448.
[6] J. Perret-Liaudet, Résonance sur-harmonique d'ordre deux dans un contact sphère-plan, *Comptes Rendus de l'Académie des Sciences* 326 (Série II-b) (1998) 787–792.
[7] T.A. Harris, *Rolling Bearing Analysis*, Wiley, New York, 1966.
[8] A. Kahraman, R. Singh, Nonlinear dynamics of a geared rotor-bearing system with multiple clearances, *Journal of Sound and Vibration* 144 (3) (1991) 469–506.
[9] B. Mehri, M. Ghorashi, Periodically forced Duffing's equation, *Journal of Sound and Vibration* 169 (3) (1994) 289–295.
[10] R.E. Mickens, Mathematical and numerical study of the Duffing-harmonic oscillator, *Journal of Sound and Vibration* 244 (3) (2001) 563–567.
[11] H. Tamura, T. Okabe, A. Sueoka, Exact solutions for free vibration in an asymmetrical Duffing equation, *JSME International Journal, Series C* 37 (1994) 260–268.
[12] K.B. Blair, C.M. Krousgrill, T.N. Farris, Harmonic balance and continuation techniques in the dynamic analysis of Duffing's equation, *Journal of Sound and Vibration* 202 (5) (1997) 717–731.
[13] K.R. Asfar, K.K. Masoud, On the period-doubling bifurcations in the Duffing's oscillator with negative linear stiffness, *Journal of Vibration and Acoustics* 114 (1992) 489–494.

[14] A.H. Nayfeh, The response of multi-degree-of-freedom systems with quadratic non-linearities to a harmonic parametric resonance, *Journal of Sound and Vibration* 90 (2) (1983) 237–244.
[15] R.A. Ibrahim, A.D.S. Barr, Parametric vibration part II: mechanics of nonlinear problems, *Shock and Vibration Digest* 10 (1978) 9–24.
[16] N. HaQuang, D.T. Mook, R.H. Plaut, A nonlinear analysis of the interactions between parametric and external excitations, *Journal of Sound and Vibration* 118 (3) (1987) 425–439.
[17] R.H. Plaut, W. Limam, Oscillations of weakly non-linear, self-excited systems under multi-frequency parametric excitation, *Journal of Sound and Vibration* 144 (2) (1991) 197–214.
[18] K. Yagasaki, Chaos in a weakly nonlinear oscillator with parametric and external resonances, *Journal of Applied Mechanics* 58 (1991) 244–250.
[19] S. Maezawa, Forced vibrations in an unsymmetric piecewise-linear system excited by general periodic force functions, *Bulletin of JSME* 23 (1980) 68–75.
[20] S.W. Shaw, P.J. Holmes, A periodically forced piecewise linear oscillator, *Journal of Sound and Vibration* 90 (1) (1983) 129–155.
[21] F.C. Moon, S.W. Shaw, Chaotic vibrations of a beam with nonlinear boundary conditions, *International Journal of Non-Linear Mechanics* 18 (1983) 465–477.
[22] S.W. Shaw, The dynamics of a harmonically excited system having rigid amplitude constraints. Part 1: subharmonic motions and local bifurcations, *Journal of Applied Mechanics* 52 (1985) 453–458.
[23] S. Natsiavas, Periodic response and stability of oscillators with symmetric trilinear restoring force, *Journal of Sound and Vibration* 132 (2) (1989) 315–331.
[24] S. Natsiavas, H. Gonzalez, Vibration of harmonically excited oscillators with asymmetric constraints, *Journal of Applied Mechanics* 59 (1992) 284–290.
[25] R.J. Comparin, R. Singh, Nonlinear frequency response characteristics of an impact pair, *Journal of Sound and Vibration* 134 (2) (1989) 259–290.
[26] A. Kahraman, R. Singh, Nonlinear dynamics of a spur gear pair, *Journal of Sound and Vibration* 142 (1) (1990) 49–75.
[27] A. Kahraman, On the response of a preloaded mechanical oscillator with a clearance: period-doubling and chaos, *Nonlinear Dynamics* 3 (1992) 183–198.
[28] Y.S. Choi, S.T. Noah, Forced periodic vibration of unsymmetric piecewise-linear system, *Journal of Sound and Vibration* 121 (1) (1988) 117–126.
[29] Y.B. Kim, S.T. Noah, Stability and bifurcation analysis of oscillators with piecewise-linear characteristics, *Journal of Applied Mechanics* 58 (1991) 545–553.
[30] S.L. Lau, W.-S. Zhang, Non-linear vibrations of piecewise linear systems by incremental harmonic balance method, *Journal of Applied Mechanics* 59 (1992) 153–160.
[31] G.W. Blankenship, A. Kahraman, Steady state forced response of a mechanical oscillator with combined parametric excitation and clearance type non-linearity, *Journal of Sound and Vibration* 185 (5) (1995) 743–765.
[32] A. Kahraman, G.W. Blankenship, Interactions between commensurate parametric and forcing excitations in a system with clearance, *Journal of Sound and Vibration* 194 (3) (1996) 317–336.
[33] S. Theodossiades, S. Natsiavas, Periodic and chaotic dynamics of motor-driven gear-pair systems with backlash, *Chaos, Solitons and Fractals* 12 (2001) 2427–2440.
[34] K. Nakamura, Tooth separations and abnormal noise on power-transmission gears, *Bulletin of JSME* 10 (1967) 846–854.
[35] K. Sato, S. Yamamoto, T. Kawakami, Bifurcation sets and chaotic states of a gear system subjected to harmonic excitation, *Computational Mechanics* 7 (1991) 173–182.
[36] V.N. Belovodsky, S.L. Tsyfansky, V.I. Beresnevich, The dynamics of a vibromachine with parametric excitation, *Journal of Applied Mechanics* 254 (2002) 897–910.
[37] A. Kahraman, R. Singh, Interactions between time-varying mesh stiffness and clearance non-linearities in geared system, *Journal of Sound and Vibration* 146 (1) (1991) 135–156.
[38] C. Padmanabhan, R. Singh, Analysis of periodically forced nonlinear Hill's oscillator with application to a geared system, *Journal of the Acoustical Society of America* 99 (1) (1996) 324–334.

[39] S. Natsiavas, S. Theodossiades, I. Goudas, Dynamic analysis of piecewise linear oscillators with time periodic coefficients, *International Journal of Non-Linear Mechanics* 35 (2000) 53–68.
[40] S. Theodossiades, S. Natsiavas, Non-linear dynamics of gear-pair systems with periodic stiffness and backlash, *Journal of Sound and Vibration* 229 (2) (2000) 287–310.
[41] R. Van Dooren, Comments on "Non-linear dynamics of gear-pair systems with periodic stiffness and backlash", *Journal of Sound and Vibration* 244 (5) (2001) 899–903.
[42] R.C. Azar, F.R.E. Crossley, Digital simulation of impact phenomenon in spur gear systems, *Journal of Engineering for Industry* (1977) 792–798.
[43] H.S. Choi, J.Y.K. Lou, Nonlinear behavior and chaotic motions of an sdof system with piecewise-non-linear stiffness, *International Journal of Non-Linear Mechanics* 26 (1991) 461–473.
[44] A. Kahraman, R. Singh, Dynamics of an oscillator with both clearance and continuous non-linearities, *Journal of Sound and Vibration* 153 (1) (1992) 180–185.
[45] Y. Wang, Dynamics of unsymmetric piecewise-linear/nonlinear systems using finite elements in time, *Journal of Sound and Vibration* 185 (1) (1995) 155–170.
[46] C. Padmanabhan, R. Singh, Dynamics of a piecewise non-linear system subject to dual harmonic excitation using parametric continuation, *Journal of Sound and Vibration* 184 (5) (1995) 767–799.
[47] A. Raghothama, S. Narayanan, Bifurcation and chaos of an articulated loading platform with piecewise non-linear stiffness using the incremental harmonic balance method, *Ocean Engineering* 27 (2000) 1087–1107.
[48] Q. Ma, A. Kahraman, Subharmonic motions of a mechanical oscillator with periodically time-varying piecewise-nonlinear stiffness, *Journal of Sound and Vibration*, in preparation.
[49] L.T. Watson, M. Sosonkina, R.C. Melville, A.P. Morgan, H.F. Walker, Algorithm 777: HOMPACK90: a suite of Fortran 90 codes for globally convergent homotopy algorithms, *ACM Transactions on Mathematical Software* 23 (4) (1997) 514–549.
[50] E.L. Allgower, K. Georg, *Numerical Continuation Methods: An Introduction*, Springer, New York, 1990.
[51] A.H. Nayfeh, B. Balachandran, *Applied Nonlinear Dynamics: Analytical, Computational, and Experimental Methods*, Wiley, New York, 1995.
[52] C.S. Hsu, W.H. Cheng, Steady state response of dynamical system under combined parametric and forcing excitations, *Journal of Applied Mechanics* (1974) 371–378.